Check for updates

# Sol–gel-assisted micro-arc oxidation synthesis and characterization of a hierarchically rough structured Ta–Sr coating for biomaterials†

Ruiyan Li, [ID] [a] Yongjie Wei, [ID] [b] Long Gu,[b] Yanguo Qin‡*[a] and Dongdong Li [ID] ‡*[b]

Tantalum (Ta) is an element with high chemical stability and ductility that is used in orthopedic biomaterials. When utilized, it can produce a bioactive surface and enhance cell–material interactions, but currently, there exist scarce effective methods to introduce the Ta element onto the surface of implants. This work reported a sol–gel-assisted approach combined with micro-arc oxidation (MAO) to introduce Ta onto the surface of the titanium (TC4) substrate. Specifically, this technique produced a substrate with a hierarchically rough structured topography and introduced strontium ions into the film. The films were uniform and continuous with numerous crater-like micropores. Compared with the TC4 sample (196 ± 35 nm), the roughness of Ta (734 ± 51 nm) and Ta–Sr (728 ± 85 nm) films was significantly higher, and both films (Ta and Ta–Sr) showed increased hydrophilicity when compared with TC4, promoting cell attachment. Additionally, the *in vitro* experiments indicated that Ta and Ta–Sr films have the potential to enhance the recruitment of cells in the initial culture stages, and improve cell proliferation. Overall, this work demonstrated that the application of Ta and Ta–Sr films to orthopedic implants has the potential to increase the lifetime of the implants. Furthermore, this study also describes an innovative strategy to incorporate Ta into implant films.

## Introduction

Musculoskeletal disorders are some of the most prevalent ailments affecting specific populations, and the age of onset became younger.[1–3] In 2010, approximately 310 800 patients (above 45 years of age) in the United States underwent total hip arthroplasty (THA).[4,5] Moreover, a 6 year study (from 2007 to 2013) demonstrated that THA revisions had significantly increased in patients between 45 and 64 years of age. This finding suggested that a large proportion of these patients will outlive their implants.[6] Therefore, developing and fabricating longer-lasting implants for this relatively young population of patients is a critical challenge.

A key factor required to achieve long-term durability of the implant is to improve the biomaterial integration with the surrounding bone tissues and cells.[7,8] Numerous studies have demonstrated that rough surfaces provide the physical cues necessary to generate synergistic effects with the chemical

signals supplied by the bio-functional composition (organic group or inorganic element). These physicochemical signals have been shown to improve osseointegration.[9] Among them, the combination of a micro-/nano-rough structure with a bio-functional metal element is a promising strategy for enhancing the integration of materials with cells or proteins.[10–12]

Among the numerous metallic biomaterials, tantalum (Ta) has attracted a lot of attention in the field of bone tissue engineering.[13–16] Ta has both high chemical stability and ductility. It has been used in clinical applications since the 1940s because it can enhance cell–material interactions, improve osteogenic differentiation of stem cells, promote the deposition of bone matrix, and ultimately improve the integration of implants and bones.[13,15,17] However, its lack of rigidity, high density, and prohibitive cost prevents its use in the manufacture of implants. Therefore, researchers have developed new methods to prepare Ta and its associated compounds as coatings for biomaterial implants. Common strategies for the preparation of Ta-based coatings for implants and scaffolds include plasma-immersion ion implantation, physical vapor deposition, and chemical vapor deposition. These methods have been optimized to fabricate biocompatibility-enhancing Ta-coated composites.[18–23] Despite this, the ion implantation and vapor deposition methods do not easily form a Ta layer over complex internal microstructures. In addition, they may also clog nanostructures such as nanopores and nanogrooves.[24] A viable
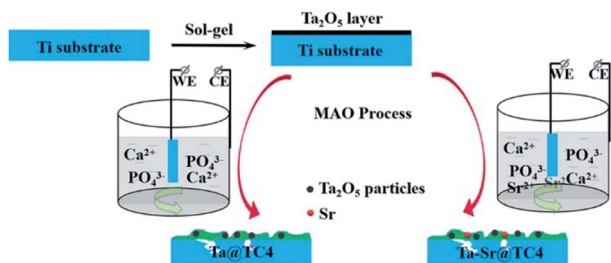
*[a]Department of Orthopedics, The Second Hospital of Jilin University, Changchun, 130041, China. E-mail: qinyanguo@hotmail.com*

*[b]Key Laboratory of Automobile Materials of MOE, Department of Materials Science and Engineering, Jilin University, Changchun 130012, China. E-mail: lidongdong@jlu.edu.cn*

‡ Yanguo Qin and Dongdong Li are co-corresponding authors.

**Scheme 1** Preparation procedure of hierarchically rough structured Ta–Sr coating on Ti substrate.

alternative strategy for preparing Ta coatings on the complex structured scaffold is the sol–gel method. The adhesion between the sol–gel coating and the substrate would affect the long-term performance and stability of the implant in the load-bearing situation in the human body.[25] Normally, the coatings produced by the sol–gel method exhibit some drawbacks that hinder its practical applications such as relative poor adhesion strength and low wear-resistance, while the coatings prepared by MAO exhibit high adhesive strength, wear resistance and corrosion resistance.[26] In our previous work, we also proved that after MAO process the bonding strength of coating with TC4 can be up to 39.4 N according to the scratch test.[27] Although the MAO technique can not be used to introduce Ta to the film alone, it could be used to enhance the mechanical properties of the sol–gel film.

In this work, $Ta_2O_5$ was incorporated into the titanium substrate by the sol–gel method and then solidified by micro-arc oxidation (Scheme 1). This sol–gel-assisted micro-arc oxidation technique resulted in a hierarchically rough structured topography on the substrate. It also provided for the possibility of the introduction of other functional ions, such as strontium (Sr), to the Ta coating. Sr is an essential trace element in human skeletal components, and numerous studies have confirmed that it promotes the proliferation and differentiation of osteoblasts, as well as the increased matrix mineralization. Additionally, *in vitro* and *in vivo* studies suggest that the Sr-doped coatings enhance bone formation.[28,29] Therefore, the doping of Sr is an efficient strategy that can be used to improve the biocompatibility of materials. The benefits of this approach are as follows: (1) The MAO technique strengthened the bonding of the coating fabricated by the sol–gel method alone; (2) the sol–gel method allowed for the introduction of Ta into the film which is difficult with the MAO technique alone; (3) the combined application of the two methods, allowed for the preparation of a coating with both Ta and Sr elements as well as a surface with a hierarchically rough structured topography. These properties contributed to the excellent integration of the biomaterial surface and cells.

# Experimental

## Materials

Ti6Al4V alloy substrates were purchased from Huitai Metal Materials Inc. of Dongguan. Tantalum(v) chloride (J&K

Scientific Ltd), $HNO_3$ (70%) (Beijing Chemical Works), phosphoric acid (Beijing Chemical Works), acetylacetone (Xilong Scientific Co., Ltd.), EtOH (Beijing Chemical Works), $H_2O_2$ (30%) (Sinopharm Chemical Reagent Co., Ltd), hydrofluoric acid (Sinopharm Chemical Reagent Co., Ltd), basal culture medium (DMEM, Gibco, USA), fetal calf serum (FCS, Tianhang Bio, Hangzhou, China), Cell-Counting Kit (CCK-8, Dojindo, Japan), phosphate-buffered solution (PBS, Daixun Bio, China), DAPI and rhodamine-phalloidin were purchased from Sigma-Aldrich LLC.

## Sol–gel deposition of tantalum oxide on titanium substrate

The sol–gel solution contained 90 ml EtOH, 2.1 ml acetylacetone, 2.5 ml nitric acid, and 5 g $TaCl_5$. After stirring for 10 min, 4 ml 30% hydrogen peroxide was added to the mixture drop by drop and mixed vigorously for 1 h at room temperature. The acquired sol–gel solution was sealed and aged for 7 days under 276 K conditions. Next, the Ti6Al4V alloy substrates were sequentially polished with a series of silicon carbide sandpapers of four grades (#400, #800, #1000 and #1500) to remove the oxides layer on the surface. Then the substrates were dip-coated in the sol–gel solution for 3 min and dried at room temperature to allow for the deposition of tantalum oxide. After that, the substrates were heated at 373 K in the oven to dry the sol–gel films completely.

## MAO modification of the substrate with Ta coating

After coating the substrate with $Ta_2O_5$ layer, further modification (using the MAO approach) was employed to incorporate Sr ions. The Ta-coated substrate was used as an anode while a stainless-steel plate was used as the cathode. Electrolyte preparation involved dissolving 3.06 g disodium beta-phosphate and 17.6 g calcium acetate in 500 ml of distilled water by ultrasonication. The experimental parameter settings were: forward voltage (350 V), negative voltage (50 V), pulse frequency (500 Hz), duty ratio (10%), and preparation time (3 min). Samples without Sr were marked as Ta@TC4, while samples with Sr were marked as Ta–Sr@TC4.

## Material characterization

Surface morphology and sample composition (before and after the deposition of Ta and Ta–Sr films) were observed by field-emission scanning electron microscopy (FE-SEM, HITACHI8010, Japan) equipped with energy-dispersive X-ray spectroscopy unit (EDS). The sample was cut into two parts by a wire cutting machine to analyze the cross-section. Then the cross-section of the sample was polished with silicon carbide sandpapers of #800 grade directly and then ultrasonically washed with acetone and distilled water to remove the contaminants. The phase composition of the layers was investigated by X-ray diffraction (XRD) measurements using a Bruker D8 ADVANCE (Cu-Kα1 radiation $\lambda = 0.1542$ nm at 40 kV and 30 mA). The surface roughness and morphologies of different samples were observed by atomic force microscopy (AFM, Bruker). Surface wettability was assessed using the pendant drop method. This method involved dropping an ultrapure water droplet with

a volume of 3.5 μl onto the specimen surface (at room temperature) and using a contact angle analyzer (DSA30, Kruess, Germany) to assess the water contact angle.

### Cell adhesion and morphology

The influence of the films (Ta and Ta–Sr) on cell adhesion and morphology was measured by counting the cell number on the sample surface. This measurement was done by performing nuclear fluorescent staining and quantifying imaged cells using ImageJ software. Briefly, the samples were placed in cell culture plates (Corning, 12-well), and seeded with MC3T3-E1 cells (1 × $10^5$ cells per well). After a 2 h culture, the cells were fixed using 4% paraformaldehyde (PFA) for 15 min, and then stained (in the dark) with DAPI (1 mM) for 5 min. Nuclei were then observed using a fluorescence microscope (Olympus, IX71, USA), and six random fields from each sample were captured and counted using ImageJ.

The cytoskeleton of cells seeded on the samples was stained to determine the effect of surface topography on cell morphology. The MC3T3-E1 cells were seeded on samples at a density of 2 × $10^4$ cells per well. After cell seeding (for 2 and 4 h), the samples with cells were washed with PBS (three times), and then fixed using 4% PFA at 4 °C for 10–20 min. Before cell staining, samples were rinsed with PBS again to remove the PFA completely. Next, rhodamine-phalloidin solution (5 μM) was added into every well, and sample incubation was performed for 50 min in the dark. The samples were then rinsed with PBS, and the nuclei were stained for 5 min with DAPI (1 mM) in the dark. Finally, images of the cytoskeleton and nuclei were captured using a confocal laser scanning microscope (CLSM, Olympus FV1000, USA). Additionally, a separate batch of cell-seeded surfaces was prepared for electron microscopy. After cell culture (2 days), the cell-seeded surfaces were washed with PBS for 5 min and fixed with 2.5% v/v glutaraldehyde in the dark (4 °C; 6–8 h). The samples were then passed through an ethanol dehydration gradient: 10 min in 30% ethanol, 10 min in 40% ethanol, 10 min in 50% ethanol, 10 min in 60% ethanol, 10 min in 70% ethanol, 10 min in 80% ethanol, 10 min in 90% ethanol, 20 min in 100% ethanol, and finally air-dried at room temperature. Lastly, samples were sputtered with a thin layer of gold before Scanning Electron Microscopy (SEM) observation (XL-30 ESEM FEG Scanning Electron Microscope FEI Company).

### Cell proliferation and viability

Surface morphology and composition are key factors that influence cell viability and proliferation. Samples ($n = 4$) were placed in cell culture plates (Corning, 12-well), then MC3T3-E1 cells were seeded on each sample at a density of 1 × $10^4$ cells per well, and culture was performed for 1, 3, and 5 days. At every time point, the cell culture medium was replaced with a mixture of DMEM and CCK-8 solution (100 : 10), and the cells were incubated at 37 °C for 2.5 h. Next, the solution in the 12-well plates was transferred to a new 96-well plate. The live cell number was assessed using the detection of absorbance at 450 nm *via* a microplate reader (Varioskan Flash, Thermo Scientific). Additionally, a separate batch of cell-seeded surfaces

was prepared for cell viability. After cell culture for 24 h, the cells on samples were stained by the Live/Dead cell staining kit, Finally, at least three random fields from each sample were captured using a fluorescence microscope (Olympus, IX71, USA).

### Statistical analysis

Each assay in this study was repeated at least three times ($n = 3$–6) for each group with parallel controls, and the data were presented as the means ± standard deviation (SD). When comparing the differences between two groups, the nonpaired Student's *t*-test was employed. We considered differences significant for a *P*-value < 0.05 (*).

## Results and discussion

Traditionally, researchers have investigated the anti-corrosion performance of titanium alloys with different types of coatings. These were prepared using the MAO method, followed by sol–gel treatment.[30,31] The pores formed during the MAO coating were effectively filled using the sol–gel treatment, which reduced the surface roughness. This finding is important to note because cellular processes such as differentiation, proliferation, and migration of human osteoblasts are dependent on the implant surface roughness. To counter this, we prepared surface coatings by first treating them with a sol–gel solution followed by MAO. The $Ta_2O_5$ particles were *in situ* solidified in the ceramic coatings under the high-temperature action of the local MAO (Scheme 1). This method did not affect the surface morphology of coatings, but it adjusted the coating composition, which resulted in a significant improvement in biomedical properties.

The morphology of TC4 and coated samples are presented in Fig. 1. It can be seen that the surface of polished TC4 (Fig. 1a, d, and g) is very flat with few nicks, which doesn't have any other rise or the appearance of micro-scale structures. In contrast to this, all the Ta@TC4 and Ta–Sr@TC4 samples had similar morphologies and rough surfaces, even though they were fabricated in different electrolyte solutions. In the 500× magnified images of Ta@TC4 and Ta–Sr@TC4 samples (Fig. 1b and c), they all showed uneven surfaces with numbers of micropores. While in the Fig. 1e and f, the films showed a porous structure morphology with numerous crater-like micropores on the surface. This complex porous structure is a feature of micro-arc coatings which are formed by micro-arc discharges and local electrical breakdown of the growing coating.[32] The images (Fig. 1h and i) of Ta@TC4 and Ta–Sr@TC4 samples demonstrate that the micropores on the films are intact and uniform both in size and distribution. Additionally, the porosity and pore size distribution of the coatings were analysed with the use of Image J software (Fig. S2†). The percentage porosity of the two coatings was similar, and the average pore size was calculated as 1.746 ± 0.922 μm, and 1.813 ± 0.992 μm for Ta@TC4 and Ta–Sr@TC4 coatings, respectively.

The SEM image and elemental mappings (Fig. 2) of the Ta–Sr@TC4 sample demonstrated the Ta–Sr@TC4 film (thickness
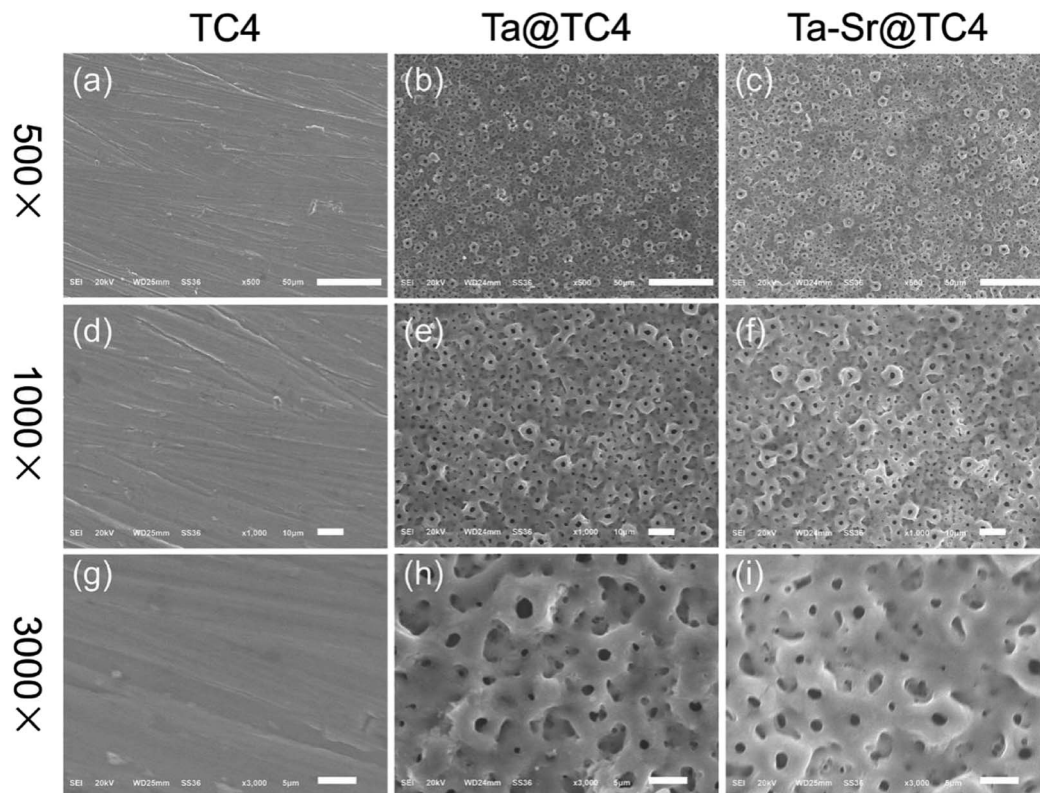
Fig. 1 The SEM micrographs of TC4 (a, d and g), Ta@TC4 (b, e, and h), and Ta–Sr@TC4 (c, f, and i) samples. Scale bar = 500×: 50 μm; 1000×: 10 μm; and 3000×: 5 μm.
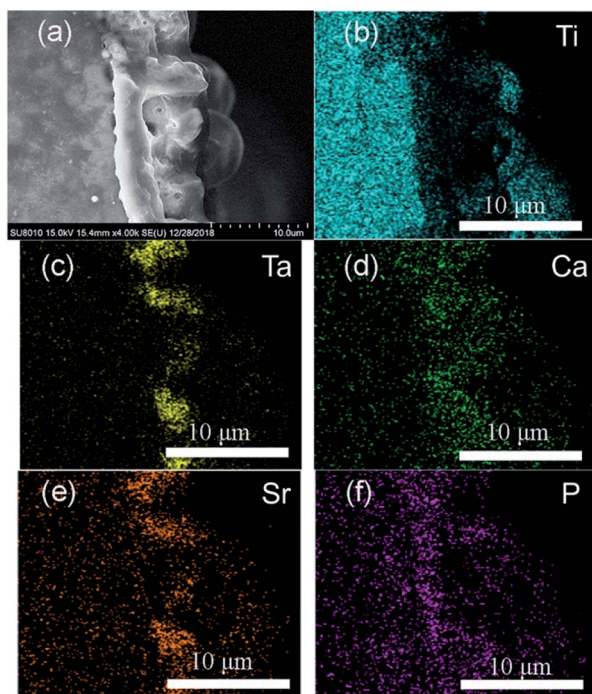


Fig. 2 Cross-sectional images of the Ta–Sr@TC4 sample (a), and elemental mappings for (b) Ti, (c) Ta, (d) Ca, (e) Sr, and (f) P.

approximately 5 μm) adhered strongly to the substrate. Moreover, the bulk and continuous film exhibited a compact morphology without cracks. The main chemical elements of the coating are Ti, O, Al, V, Ta, Ca, Sr, and the elemental mappings for the Ti, Ta, Ca, Sr, and P are shown in Fig. 2b–f. Sr from the electrolyte and Ta from the sol–gel, distribute in the outer layer of the substrate, which indicates that the bio-functional metal elements were successfully introduced. The Sr was introduced into the coating by MAO method following the reaction mechanism:

$$TiO_2 + Sr^{2+} + 2OH^- \rightarrow SrTiO_3 + H_2O$$

The phase structure of TC4 before and after coating was analyzed by XRD (Fig. 3). For sample TC4, the diffraction peak corresponds with the standard diffraction peaks of TC4. After the MAO process, anatase and rutile diffraction peaks at $2\theta = 25.3°, 27.5°$ are present, which conform with JCPDS 96-900-7433. To complement these findings, an EDS analysis was performed to determine the coating composition. The results show that the Ta, Sr, Ca, and P elements are uniformly distributed on the surface of coatings (Fig. S2†). The Ta and Sr concentrations on the surface of Ta–Sr@TC4 are approximately 5.86 and 1.93 wt%, respectively. The introduction of Ta and Sr into coatings may accelerate the formation and calcification of bone tissue, thereby reducing fracture healing time.[33,34]
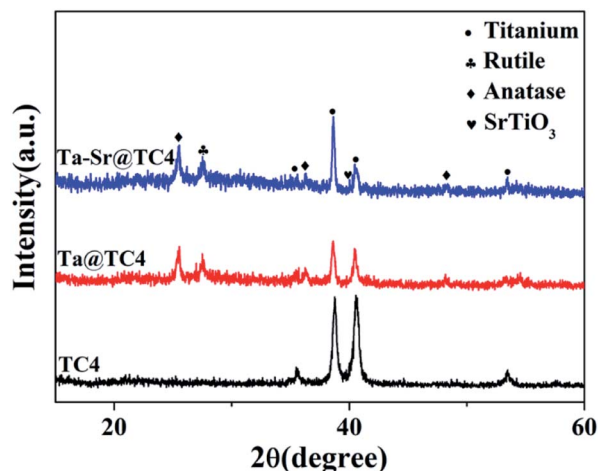
**Fig. 3** The X-ray diffraction of Ta–Sr@TC4, Ta@TC4, and TC4 samples.

Surface roughness plays a major role in influencing cell–material interactions, and rough surfaces promote adhesion better than smooth surfaces. Atomic Force Microscopy (AFM) was used to quantify the surface morphology of the coatings and to measure pore roughness precisely. After treatment with MAO, the surface roughness changed with the morphology. The average roughness (Fig. 4) was found to be: TC4 ($196 \pm 35$ nm), Ta@TC4 ($734 \pm 51$ nm), and Ta–Sr@TC4 ($728 \pm 85$ nm). This result indicated that the Ta@TC4 and Ta–Sr@TC4 samples had relatively rougher surfaces compared with the TC4 sample, and this may contribute to enhanced *in vivo* bone integration and implant stability.

A critical factor in determining the biocompatibility of a substrate is the surface energy. The water contact angle is the primary marker of the surface energy, where a lower water contact angle means higher surface energy.[35,36] Therefore, the water contact angles for the TC4 substrate, Ta@TC4, and Ta–Sr@TC4 samples were measured (Fig. 5). The water contact angles were as follows: TC4 ($68.4 \pm 1.6°$), Ta@TC4 ($37.4 \pm 0.8°$)
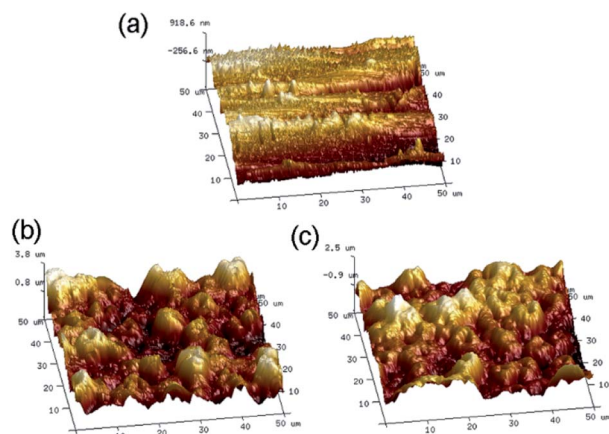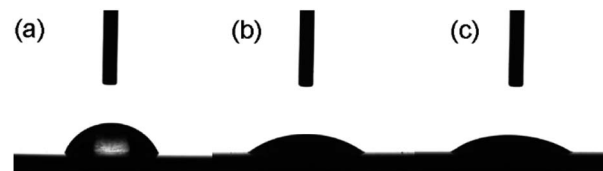


**Fig. 5** The water contact angle of the TC4, Ta@TC4, and Ta–Sr@TC4 samples.

and Ta–Sr@TC4 ($34.7 \pm 2.6°$). It is clear that as compared with the TC4 substrate, the surface energy of the coated substrate increased because of a reduced water contact angle. A higher surface energy substrate (better wettability) would enhance cell recruitment and adhesion.

To evaluate the cell recruitment ability of the films (Fig. 6), the nuclei of the cells on different samples were stained and counted after cell seeding for 2 h. As shown in Fig. 6a–c, a large number of nuclei (blue, DAPI-stained) were observed on all the samples, with a higher density of cells (quantified using ImageJ) on the Ta@TC4 and Ta–Sr@TC4 samples relative to the TC4 group. The number of cells adhered to different samples ranged from Ta–Sr@TC4 (highest), Ta@TC4 (middle), and TC4 (lowest). This result indicates that Ta@TC4 and Ta–Sr@TC4 films with hierarchically rough structures can recruit cells onto the surface of implants in the initial culture stages.

The ideal biomaterial should not only recruit cells from the surrounding microenvironment but also provide a suitable interface for cell attachment, spreading, and migrating.[37] Therefore, the cytoskeleton of cells seeded on different samples was stained and imaged to analyze the effect of the film surface on cell attachment and spreading (Fig. 7a). Within 2 h of culture, all cells were round and had a shrunken cell morphology. After 4 h, the cells gradually spread better on all the sample surfaces. On Ta@TC4 and Ta–Sr@TC4 samples, cells were fusiform and had an expanding cell morphology, which was in contrast to cells on the surface of the TC4 sample
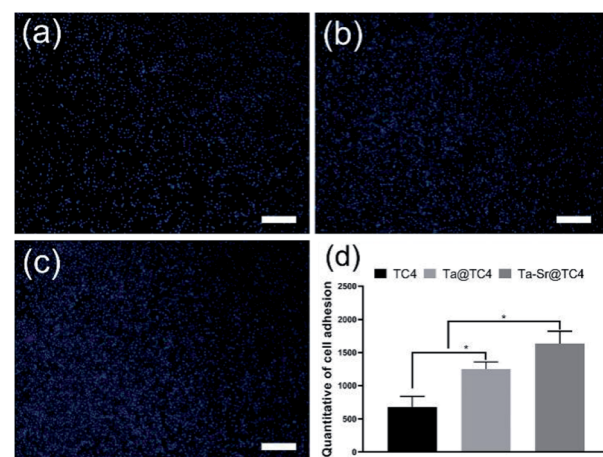


**Fig. 4** The AFM images and the roughness for the TC4, Ta@TC4 and Ta–Sr@TC4 samples.



**Fig. 6** The fluorescent staining images of nuclei for TC4 (a), Ta@TC4 (b) and Ta–Sr@TC4 (c) samples. Scale: 500 μm. The quantitative of cell adhesion after cell seeding for 2 h (d).
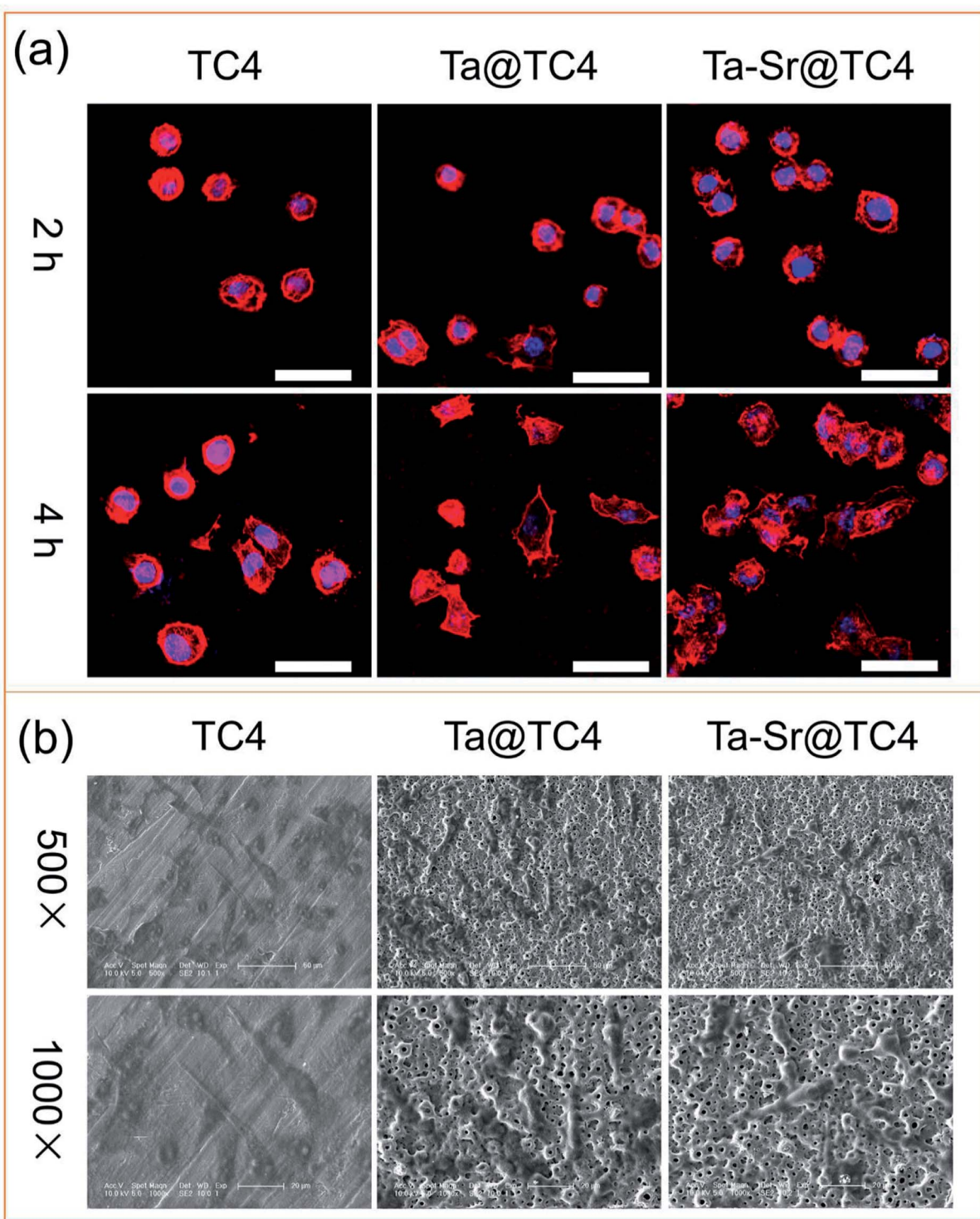
**Fig. 7** (a) The CLSM images of F-actin and nuclei of cells on the TC4, Ta@TC4, and Ta−Sr@TC4 samples. Scale: 50 μm. (b) The SEM images of the cells on different samples.

that maintained a shrunken morphology. Additionally, cell filaments were observed on the TC4 group at 4 h, while a negligible number of filaments were visualized in other groups. This behavior suggests that the cells were tightly attached to the hierarchically rough structure of the samples.

Making it difficult to image (focus and capture) a whole cell that is not on the same plane. To directly observe the interaction between cells and the surface of the materials, the SEM images for cells on different samples were captured after culture for 2 days (Fig. 7b). Numerous cells were observed on the surfaces of

different samples, and they all displayed a fusiform-expanding cell morphology. Compared with the TC4 group, cells adhered to the Ta@TC4 and Ta–Sr@TC4 films showed a more stereoscopic morphology caused by the hierarchically rough structure. The cell cytoskeleton completely covered the microcraters, and this demonstrates that the hierarchically rough structure is beneficial for cell anchorage.[29] The results of the fluorescently-labeled cytoskeleton images, as well as SEM images of cells seeded on different samples reveal that the hierarchically rough structure of Ta@TC4 and Ta–Sr@TC4 films can induce cell attachment and spreading onto the surface of the implant.

Both Live/Dead and proliferation assays were used to evaluate the cytotoxicity of the different films seeded with MC3T3-E1 cells (Fig. 8). Fig. 8a–c showed the CLSM images of the MC3T3-E1 cells cultured on the TC4, Ta@TC4, and Ta–Sr@TC4 groups for 24 h. The live cells (green dots) and dead cells (red dots) were stained and quantified. A large number of live cells and few dead cells were observed on the surface of all the samples.

Cell proliferation (assayed using the CCK-8 kit) is important for understanding cell–material interactions (Fig. 8d). The OD value (indicating cell number) of all sample groups increased with incubation time. After 1 day of seeding, the number of cells on all samples was almost similar. While at 3 days, the Ta–Sr@TC4 group had a higher amount of cells, and 5 days post-seeding, there were more cells in both the Ta@TC4 and Ta–Sr@TC4 groups compared with the TC4 group. Based on the results of the Live/Dead staining and cell proliferation assay, we conclude that the Ta@TC4 and Ta–Sr@TC4 films are conducive for cell growth compared with the TC4 group. Previous studies demonstrate that functional elements such as Sr and Ta can enhance both cell proliferation and the osteoblastic response.[38,39] However, in this work, the doping of the functional elements is not the sole factor responsible for the enhanced cell response. The Ta@TC4 and Ta–Sr@TC4 films demonstrated the ability to recruit cells onto the surface in the initial culture stages. This cell recruitment is closely related to the surface morphology and substrate cell affinity. The interaction of cells with various surface topographies also influences cell proliferation. It has been reported that the complex porous structure of the micro-arc coatings could provide a conducive environment for cell adhesion and migration.[40] Therefore, the synergistic strategy combining both functional elements and porous surface topography contributes to the improved cell proliferation on Ta@TC4 and Ta–Sr@TC4 films.

## Conclusions

In this study, uniform and continuous Ta@TC4 and Ta–Sr@TC4 films were successfully prepared on the TC4 substrates using the sol–gel-assisted micro-arc oxidation method. The introduction of tantalum was caused by the disposition of $Ta_2O_5$ sol–gel. At the same time, the MAO technique introduced Sr ions and created a hierarchically rough structured topography with a large number of crater-like micropores. Moreover, the MAO technique enhanced the bond strength of the films and the surface. The hierarchically porous surface provided by the Ta and Ta–Sr films was rougher and more hydrophilic relative to the TC4 substrate (a feature beneficial for cell attachment). Altogether, both films were biocompatible, and they enhanced cell proliferation. Based on these results, the sol–gel-assisted micro-arc oxidation method is a novel strategy for the introduction of Ta to implant films. This feature makes it a great approach for fabricating bioactive coatings on implants and scaffolds for bone repair and regeneration.

## Conflicts of interest

The authors declare that the research was conducted in the absence of any commercial or financial relationships that could be construed as a potential conflict of interest.

## Acknowledgements

Fig. 8 The images of Live/Dead cell staining of MC3T3-E1 cells on the TC4 (a), Ta@TC4 (b), and Ta–Sr@TC4 (c) samples. Scale: 500 μm. The proliferation of the cells on different samples after culture for 1, 3, and 5 days (d).

## Notes and references

1 D. G. Hoy, E. Smith, M. Cross, L. Sanchez-Riera, F. M. Blyth, R. Buchbinder, A. D. Woolf, T. Driscoll, P. Brooks and L. M. March, *Ann. Rheum. Dis.*, 2015, **74**, 4–7.

2 S. Bevan, *Best Pract. Res., Clin. Rheumatol.*, 2015, **29**, 356–373.

3 A. Sargeant and T. Goswami, *Mater. Des.*, 2006, **27**, 287–307.

4 D. Ke, A. A. Vu, A. Bandyopadhyay and S. Bose, *Acta Biomater.*, 2019, **84**, 414–423.

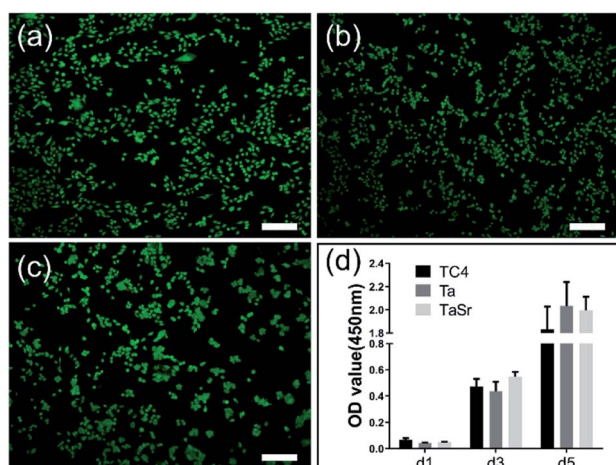5 M. Wolford, K. Paso, A. Bercovitz, *United States NCHS Data Brief*, 2015, p. 186.

6  S. S. Rajaee, J. C. Campbell, J. Mirocha and G. D. Paiement, *J. Bone Jt. Surg.*, 2018, **100**, 449–458.

7  M. A. Fernandez-Yague, S. A. Abbah, L. McNamara, D. I. Zeugolis, A. Pandit and M. J. Biggs, *Adv. Drug Delivery Rev.*, 2015, **84**, 1–29.

8  S. R. Frenkel, J. Simon, H. Alexander, M. Dennis and J. L. Ricci, *J. Biomed. Mater. Res.*, 2002, **63**, 706–713.

9  F. J. O'brien, *Mater. Today*, 2011, **14**, 88–95.

10 Y. Zhu, K. Zhang, R. Zhao, X. Ye, X. Chen, Z. Xiao, X. Yang, X. Zhu, K. Zhang and Y. Fan, *Biomaterials*, 2017, **147**, 133–144.

11 T. Gong, J. Xie, J. Liao, T. Zhang, S. Lin and Y. Lin, *Bone Res.*, 2015, **3**, 15029.

12 L. Xia, N. Zhang, X. Wang, Y. Zhou, L. Mao, J. Liu, X. Jiang, Z. Zhang, J. Chang and K. Lin, *J. Mater. Chem. B*, 2016, **4**, 3313–3323.

13 D. Cristea, I. Ghiuta and D. Munteanu, *Bull. Transilvania Univ. Brasov, Ser. I*, 2015, **8**, 151.

14 M. Niinomi, M. Nakai and J. Hieda, *Acta Biomater.*, 2012, **8**, 3888–3903.

15 R. Wauthle, J. Van Der Stok, S. A. Yavari, J. Van Humbeeck, J.-P. Kruth, A. A. Zadpoor, H. Weinans, M. Mulier and J. Schrooten, *Acta Biomater.*, 2015, **14**, 217–225.

16 C. Mas-Moruno, B. Garrido, D. Rodriguez, E. Ruperez and F. J. Gil, *J. Mater. Sci.: Mater. Med.*, 2015, **26**, 109.

17 W. T. Huo, L. Z. Zhao, S. Yu, Z. T. Yu, P. X. Zhang and Y. S. Zhang, *Sci. Rep.*, 2017, **7**, 40868.

18 S. Du, K. Zhang, M. Wen, Y. Qin, R. Li, H. Jin, X. Bao, P. Ren and W. Zheng, *Vacuum*, 2018, **150**, 222–231.

19 X. Li, L. Wang, X. Yu, Y. Feng, C. Wang, K. Yang and D. Su, *Mater. Sci. Eng., C*, 2013, **33**, 2987–2994.

20 B. Rahmati, A. A. Sarhan, W. J. Basirun and W. Abas, *J. Alloys Compd.*, 2016, **676**, 369–376.

21 J. Xu, L. Liu, P. Munroe and Z.-H. Xie, *J. Mater. Chem. B*, 2015, **3**, 4082–4094.

22 C. Park, Y.-J. Seong, I.-G. Kang, E.-H. Song, H. Lee, J. Kim, H.-D. Jung, H.-E. Kim and T.-S. Jang, *ACS Appl. Mater. Interfaces*, 2019, **11**, 10492–10504.

23 C. Park, S.-W. Lee, J. Kim, E.-H. Song, H.-D. Jung, J.-U. Park, H.-E. Kim, S. Kim and T.-S. Jang, *Biomater. Sci.*, 2019, **7**(7), 2907–2919.

24 R. Li, Y. Qin, G. Liu, C. Zhang, H. Liang, Y. Zhang and K. Zhang, *RSC Adv.*, 2017, **7**, 55408–55417.

25 M. May, H. Wang and R. Akid, *J. Coat. Technol. Res.*, 2013, **10**, 407–413.

26 T. H. Qaid, S. Ramesh, F. Yusof, W. J. Basirun, Y. C. Ching, H. Chandran and S. Krishnasamy, *Ceram. Int.*, 2019, **45**, 18371–18381.

27 Y. Wei, Y. Hu, M. Li and D. Li, *Surf. Eng.*, 2020, 1–8.

28 C.-J. Chung and H.-Y. Long, *Acta Biomater.*, 2011, **7**, 4081–4087.

29 S. Wang, R. Li, D. Li, Z.-Y. Zhang, G. Liu, H. Liang, Y. Qin, J. Yu and Y. Li, *J. Mater. Chem. B*, 2018, **6**, 3254–3261.

30 M. Bayati, H. Zargar, A. Talimian, A. Ziaee and R. Molaei, *Surf. Coat. Technol.*, 2010, **205**, 2483–2489.

31 W. Shang, B. Chen, X. Shi, Y. Chen and X. Xiao, *J. Alloys Compd.*, 2009, **474**, 541–545.

32 M. B. Sedelnikova, E. G. Komarova, Y. P. Sharkeev, A. V. Ugodchikova, L. S. Mushtovatova, M. R. Karpova, V. V. Sheikin, L. S. Litvinova and I. A. Khlusov, *Surf. Coat. Technol.*, 2019, **369**, 52–68.

33 W. Zhang, H. Cao, X. Zhang, G. Li, Q. Chang, J. Zhao, Y. Qiao, X. Ding, G. Yang and X. Liu, *Nanoscale*, 2016, **8**, 5291–5301.

34 L.-Y. Shi, A. Wang, F.-Z. Zang, J.-X. Wang, X.-W. Pan and H.-J. Chen, *Colloids Surf., B*, 2017, **160**, 22–32.

35 J. Rosales-Leal, M. Rodríguez-Valverde, G. Mazzaglia, P. Ramón-Torregrosa, L. Díaz-Rodríguez, O. García-Martínez, M. Vallecillo-Capilla, C. Ruiz and M. Cabrerizo-Vílchez, *Colloids Surf., A*, 2010, **365**, 222–229.

36 M. Pegueroles, C. Aparicio, M. Bosio, E. Engel, F. Gil, J. Planell and G. Altankov, *Acta Biomater.*, 2010, **6**, 291–301.

37 R. A. Marklein and J. A. Burdick, *Adv. Mater.*, 2010, **22**, 175–189.

38 X. Lin, X. Yang, L. Tan, M. Li, X. Wang, Y. Zhang, K. Yang, Z. Hu and J. Qiu, *Appl. Surf. Sci.*, 2014, **288**, 718–726.

39 R. Li, G. Liu, L. Yang, X. Tang, D. Guo, K. Zhang and Y. Qin, *J. Biomed. Mater. Res., Part A*, 2020, 1–10.

40 X. Yang, M. Li, X. Lin, L. Tan, G. Lan, L. Li, Q. Yin, H. Xia, Y. Zhang and K. Yang, *Surf. Coat. Technol.*, 2013, **233**, 65–73.